I&EC research
Industrial & Engineering Chemistry Research

pubs.acs.org/IECR

Article

Water-Based Scalable Methods for Self-Cleaning Antibacterial ZnO-Nanostructured Surfaces

Athanasios Milionis,[§] Abinash Tripathy,[§] Matteo Donati, Chander Shekhar Sharma, Fei Pan, Katharina Maniura-Weber, Qun Ren, and Dimos Poulikakos*

Cite This: *Ind. Eng. Chem. Res.* 2020, 59, 14323−14333

Read Online

ACCESS | Metrics & More | Article Recommendations | Supporting Information

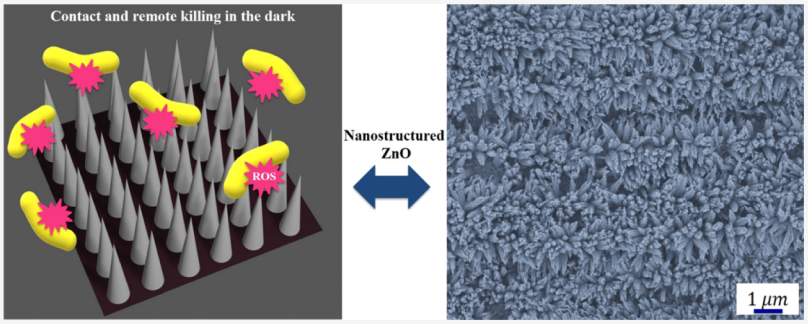

ABSTRACT: Bacterial colonization poses significant health risks, such as infestation of surfaces in biomedical applications and clean water unavailability. If maintaining the surrounding water clean is a target, developing surfaces with strong bactericidal action, which is facilitated by bacterial access to the surface and mixing, can be a solution. On the other hand, if sustenance of a surface free of bacteria is the goal, developing surfaces with ultralow bacterial adhesion often suffices. Here we report a facile, scalable, and environmentally benign strategy that delivers customized surfaces for these challenges. For bactericidal action, nanostructures of inherently antibacterial ZnO, through simple immersion of zinc in hot water, are fabricated. The resulting nanostructured surface exhibits extreme bactericidal effectiveness (9250 cells cm^{-2} h^{-1}) that eliminates bacteria in direct contact and also remotely through the action of reactive oxygen species. Remarkably, the remote bactericidal action is achieved without the need for any illumination, otherwise required in conventional approaches. As a result, ZnO nanostructures yield outstanding water disinfection of >99.98%, in the dark, by inactivating the bacteria within 3 h. Moreover, Zn^{2+} released to the aqueous medium from the nanostructured ZnO surface have a concentration of 0.73 ± 0.15 ppm, markedly below the legal limit for safe drinking water (5−6 ppm). The same nanostructures, when hydrophobized (through a water-based or fluorine-free spray process), exhibit strong bacterial repulsion, thus substantially reducing bacterial adhesion. Such environmentally benign and scalable methods showcase pathways toward inhibiting surface bacterial colonization.

1. INTRODUCTION

Bacterial contamination of common surfaces and drinking water has been traditionally the main infection routes for transmission of serious diseases, often leading to mortality. The most relevant example of surface contamination is healthcare-associated infections (HAI), which occur in hospitalized environments. These HAIs are generally transmitted through contaminated surgical tools, medical devices, and improper active disinfection. Specifically, the probability of infection in hospitalized patients is 7−10% in developing countries, while in intensive care units, this probability rises to 30%, even in high-income countries.[1] Additionally, recent research is pointing out that there is growing antibiotic resistance of pathogens in hospitalized patients.[2−4] Methicillin-resistant *Staphylococcus aureus* is a characteristic example because its treatment is still a significant challenge worldwide.[5−8] Using smart antibacterial materials in hospitals could halt the transmission of such pathogens.

Bacterial contamination of drinking water is a result of insufficient sanitation throughout the world, more pronounced in Southeast Asian and African countries. It is expected to become worse in the future because of the global increase of water scarcity. Approximately two-thirds of the global population encounters severe water crisis at least for one month a year.[9] Additionally, 30% of the population does not have easy access to clean drinking water and 20% of deaths

Received: April 20, 2020
Revised: July 5, 2020
Accepted: July 7, 2020
Published: July 7, 2020

https://dx.doi.org/10.1021/acs.iecr.0c01998
Ind. Eng. Chem. Res. 2020, 59, 14323−14333

among younger than five-year old children is due to water-related diseases.[10] The gravity of this situation requires low-cost solutions to disinfect water, while ensuring the minimum use of chemicals to protect health and the environment.

A logical strategy to combat bacterial contamination on surfaces passively is to fabricate surfaces which minimize bacterial adhesion through appropriate micro/nanoengineering and surface chemical treatment (anti-biofouling approach).[11,12] Such surfaces are capable of passive self-cleaning, the most popular example found in nature being the Lotus leaf.[13−15] They can be superhydrophobic, exhibiting static water contact angles greater than 150° and contact angle hysteresis (CAH) less than 10°. The disadvantage of such surfaces is that, although they ensure low adhesion of various liquid and solid substances, they are not designed to kill bacteria and they will likely show contamination with time and require periodic cleaning or replacement.

An alternative approach is to employ materials that can cause the death of bacteria (bactericidal approach). Here, either direct contact with bacteria is needed or the activation of a reactive oxygen species (ROS) reaction. These ROS can be efficiently transported through the water medium, reaching the bacteria in close proximity with the substrate, and killing them.[16−18] An example of naturally occurring bactericidal surfaces, featuring contact mechanical killing through impalement on the surface nanostructures, is the cicada wings.[19] However, in this type of surfaces, unless the dead bacteria are washed off naturally or artificially, they will stay adhered to the surface, gradually forming a fouling layer detrimental to surface performance.

Here, we explore zinc oxide, a common semiconducting material, which is both antibacterial and cytocompatible.[20,21] Different theories have been proposed to explain its intrinsic antibacterial properties arising from molecular mechanisms such as the generation of Zn ions,[22] the generation of ROS,[21] and the inhibition of other metal ions that are of vital importance for bacteria.[23] There is still ongoing research to fully understand ZnO interactions with bacteria.[24,25]

In addition to its bactericidal property, a ZnO surface can also be nanostructured by using chemical etching, similar to other metals such as copper and aluminium,[26] which can enhance its antimicrobial properties.[20,21,27] Chemical etching is easily scalable[28] similar to other approaches for surface structuring of metals such as anodization,[29] coating application by spray[30] or immersion,[31] and laser-based methods.[32] However, it typically requires using hazardous chemicals such as strong acids and carcinogenic solvents, while a subsequent surface coating is also needed, typically involving the use of biopersistent polymers.[33,34] A few approaches using hot water baths to create nanostructures directly on metals have been reported.[35−37] However, the requirement of subsequent deposition of a hydrophobic layer (often requiring flammable or toxic solvents[38]) compromises the sustainability of these materials. Alternative green fabrication approaches that have been proposed apply liquid-repellent coatings on metallic surfaces by spraying water-based, nanocomposite dispersions.[30,39,40] This approach, however, produces a coating of several microns thick, with an inherent micro/nano-topography, which fully covers the metallic substrate texture.

In addition to passive antibacterial methods involving low bacterial adhesion or bactericidal action, there are also some semi-passive methods against bacterial contamination, activated by an external stimulus (*e.g.*, light). Solar water disinfection (SODIS) is an efficient process to disinfect water because waterborne pathogens are inactivated when exposed to sunlight.[41] UVA rays play an important role in the formation of ROS in water, which damage the DNA of the microbes and inactivate them.[42] Increasing temperature of water because of sunlight also contributes to the failure of DNA repair mechanism of pathogens. The effectiveness of this process depends on the intensity and absorption of the sunlight. Hence, containers of contaminated water need to be transparent and exposed to sunlight for 6−48 h for disinfection.[41,43] As a result, this approach is severely limited during cloudy weather and cannot be effective during night.

Here, we demonstrate that nanostructured ZnO surfaces, fabricated by a fully water-based protocol, present scalable and customized pathways to tackle bacterial contamination of surfaces and drinking water. When used as is, ZnO nanostructures demonstrate significantly enhanced bactericidal action, both on the surface itself as well as remotely, and most importantly, in the absence of sunlight. Subsequently, we show that nanostructured ZnO is able to disinfect contaminated water while easily satisfying the strict legal limits on zinc ion concentration. Next, using the same ZnO nanostructures and adding a second hydrophobization step, also fully water-based, we obtain superhydrophobic, self-cleaning surfaces with minimal bacterial adhesion, which can potentially mitigate bacterial contamination. The hydrophobization is achieved either by deposition of a highly conformal, biodegradable, and water-soluble fluoroalkylsilane (FAS) or ethanol-soluble stearic acid (SA). We characterize quantitatively all the aforementioned surfaces with respect to bactericidal and self-cleaning properties. The resulting impressive and tunable antibacterial behavior, combined with its inherently "green" and scalable fabrication method, could render these materials to be excellent candidates in sustainable antibacterial and water purification applications.

2. MATERIALS AND METHODS

2.1. Materials. Thick zinc sheets (1 mm) of 99.9% purity were purchased from Klöckner & Co, Germany, and used as substrates. The FAS with the trademark "Dynasylan SIVO 121" was provided by Evonik, Germany. SA was purchased from Sigma-Aldrich. All solvents used were of analytical grade. All media and chemical reagents used for bacterial assays were purchased from Sigma-Aldrich (Buchs, Switzerland) and applied as received unless otherwise noted. Phosphate-buffered saline (PBS) at pH 7.4 was prepared as following: 8 $g{\cdot}L^{-1}$ NaCl, 0.2 $g{\cdot}L^{-1}$ KH_2PO_4, and 1.44 $g{\cdot}L^{-1}$ Na_2PO_4 in distilled water.

2.2. Sample Preparation and Nanostructuring. Zinc samples were thoroughly cleaned with acetone and isopropyl alcohol using ultrasonic processing in order to minimize the presence of organic contaminants prior to fabrication. Subsequently, glass beakers filled with deionized water were heated using a hotplate until the temperature of the water reached 95 °C. At that point, the temperature was maintained fixed using a thermocouple and the zinc samples were placed inside the hot water. The exposure time of the samples inside the hot water varied from 30 min to 1 day, and the surface nanotexture was examined afterward.

2.3. Surface Hydrophobization with FAS. The nanostructured samples were hydrophobized by spraying water-based solutions with different FAS concentration. The spray was performed using a VL double action, internal mix, siphon

https://dx.doi.org/10.1021/acs.iecr.0c01998
Ind. Eng. Chem. Res. 2020, 59, 14323−14333

feed airbrush (Paasche, USA). The spray distance was held constant at approximately 15 cm, and the air pressure was set at 300 kPa. The concentration of FAS in water varied from 0.5 to 10 wt %. The optimum concentration of FAS was found to be 1 wt %. The samples were sprayed in steps of 4 s each, with drying intervals of 10 s between each spray cycle in order to allow for sufficient time for the solvent (water) evaporation. During the spraying process, the samples were placed on a hotplate maintained at a constant temperature of 200 °C in order to facilitate water evaporation. Finally, before proceeding to any measurements, the samples were left to dry for 5 min at ambient conditions.

2.4. Surface Hydrophobization with Stearic Acid. As an alternative hydrophobization approach, the nanostructured samples were immersed for 6 min in ethanolic SA solutions. The concentrations of these solutions varied from 0.2 to 10 mM. The optimum concentration of SA was found to be 0.38 g/L. After the immersion, the SA-coated samples were left on a hotplate at 140 °C, markedly above the melting point of SA (69−71 °C), for 15 min in order to melt the SA and force it to conform to the nanostructured substrate topography.

2.5. Wetting Measurements. Static and dynamic contact angles on the surfaces were measured by a video-based optical contact angle measuring instrument OCA 35 Dataphysics, Germany. Deionized water drops (5 μL) were gently placed on the surfaces, and the static contact angles were measured. Advancing and receding angles were measured by dispensing and retracting liquid volume until a motion of the three-phase contact line was observed. The arithmetic value of the difference between the advancing and receding contact angles (RCAs) was reported as CAH. For all the aforementioned measurements, at least three independent measurements were conducted in different locations and the standard deviation was also calculated.

2.6. Scanning Electron Microscopy Measurements. The morphology of the textured surfaces was characterized by a Hitachi SU8200, Japan. The FEI Quanta 600 ESEM equipped with a gaseous back scattered electron detector was used to study droplet nucleation and growth on the superhydrophobic surfaces. The sample temperature was controlled through a Peltier cooling stage (Emott AG). The samples were mounted using custom made copper stubs that allowed imaging at beam incidence angles of 45 and ∼87.5°. In order to minimize the beam heating effects, a beam voltage of 20 kV and a spot current of 0.16 nA were used and the viewing area was kept above 100 μm × 100 μm for all the experiments.[44] The cooling stage was set to 2 °C, and the chamber pressure was slowly increased until the onset of condensation, following which the chamber pressure was kept constant in the range of 0.7−0.8 kPa.

For studying the morphology of the bacteria located on the surface of the test samples, fixing of bacteria was carried out using Kanovsky-fixing solution [100 mL contains 11 mL 4% paraformaldehyde (Sigma 30525), 49 mL DI water (60 °C preheated + 2−6 drops 1 M NaOH, till the solution is clear), 10 mL 2.5% glutaraldehyde (Sigma G5882), 45 mL 1× PBS, pH = 7.4] followed by dehydration with ethanol (30 min in 50%, 30 min in 70%, 30 min in 80%, 60 min in 90%, and 60 min in 100%). After that, samples were placed in hexamethyldisilazane (HMDS, Sigma 440191)-filled wells and incubated for 30 min at room temperature. Post incubation, HMDS was removed with a pipette and samples were dried in blank wells at room temperature. Prior to scanning electron microscopy (SEM) imaging, coating of 5 nm of platinum was performed to avoid charging of the samples.

2.7. Self-Cleaning Experiments. The self-cleaning properties of the samples were evaluated by taking videos with artificial contaminants, in order to capture in detail the contamination removal upon drop-rolling motion on the surfaces. Sudan II (Sigma Aldrich) powder was spread all over the sample's surface to simulate the presence of a contaminant. The sample was then placed in an inclined position (<5°), and water drops were carefully dispensed close to the surface of the sample in order to minimize the effect of drop impact on the surface.

2.8. Bacterial Viability Experiment. The antibacterial test was performed on four substrates: silicon, flat zinc, superhydrophilic nanostructured ZnO, and superhydrophobic nanostructured ZnO (SA coated). A 24-well plate was used, and sample size was 1 cm × 1 cm. *Escherichia coli* DSMZ 30083 preculture was prepared in 20 mL 30% TSB with 0.25% glucose and incubated overnight at 37 °C and 160 rpm. The pre-culture was diluted to optical density (O.D.) 600 nm of 0.1 and inoculated in 30% TSB with 0.25% glucose for 1.5 h at 37 °C and 160 rpm to obtain mid-exponentially growing cells, which were then diluted to O.D. 600 nm of 0.01 in 0.9% NaCl for following interaction experiments with the fabricated materials. This bacterial suspension (2 mL) was loaded onto the test surfaces at room temperature and incubated at 37 °C for 3 h without shaking. After incubation, the cell suspension was removed by aspirating the liquid and the tested samples were washed two times with 1 mL of 0.9% NaCl to remove the nonadhered cells. The suspension and the washing solution were combined and the mixture was evaluated by classical colony counting method.[45] From each dilution step of the bacterial suspension, 5 μL aliquots were pipetted onto one Plate-Count-Agar plate. Plates were incubated at 37 °C for 16 h. Colonies were counted, and the number of colony forming units (CFUs) per mL of the original sample was calculated. To release the adhered cells from the tested samples for viable cell quantification, the substrates were placed into a 50 mL Falcon tube containing 2.5 mL of PBS and sonicated for 5 min in an ultrasonication water−ice bath (Bransonic 52, Branson Ultrasonics SA, Carouge, Switzerland) at a frequency of 40 kHz and room temperature, followed by further vortexing for 15 s. The released bacterial cells from the surfaces were then analyzed by the classical colony counting method.[45]

2.9. ROS Quantification. Flat zinc, superhydrophilic nanostructured ZnO, superhydrophobic nanostructured ZnO (SA coated), and superhydrophobic nanostructured ZnO (FAS coated) samples were placed in a 24-well plate in triplicates (*i.e.,* 3 from each sample); 2 mL of DI water was added to each well with the samples (flat zinc and nanostructured ZnO surface). In addition, 2 mL of DI water was added to three other wells with no samples, which were used as controls; 100 μL of 10 μM Dihydrorhodamine 123 (DHR123, Sigma Aldrich) was added to the wells in dark condition. Then, immediately, the fluorescence reading (using Synergy H1 multimode microplate reader) at zero time point was taken from each well. After that, the well plate was wrapped with aluminium foil and kept in dark. Subsequently, the fluorescence readings of all the substrates including the blank wells were obtained at 0.5, 1, 3, 8, and 24 h.

Zn^{2+} ion concentration in PBS medium was quantified using high-resolution ICP−MS (Thermo Fisher Scientific) instrument. A standard zinc solution (1 ppb, Thermo Fisher

https://dx.doi.org/10.1021/acs.iecr.0c01998
Ind. Eng. Chem. Res. 2020, 59, 14323−14333

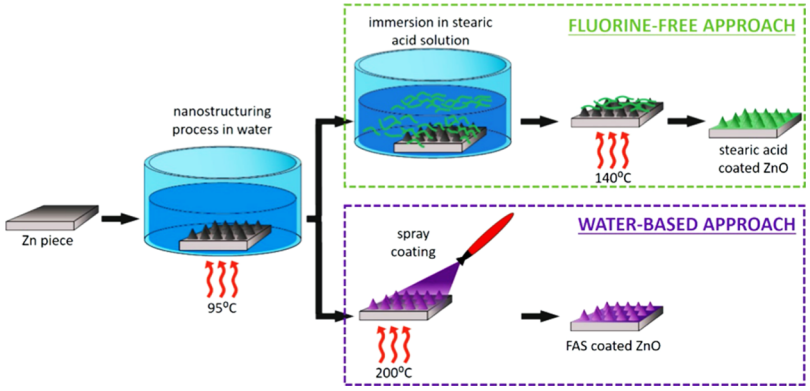

Figure 1. Sketch depicting the fabrication strategies for nanostructuring and hydrophobization used in this work. The Zn substrate is nanostructured with ZnO in hot water for several hours. As a second step, either a fluorine-free immersion process in ethanolic SA solution with an additional annealing step (green box) or a water-based spray coating process with a readily degradable FAS as the hydrophobization compound (purple box) can be adopted.

Scientific) was used to get the standard calibration plot by measuring the zinc ion concentration. Flat zinc, superhydrophilic nanostructured ZnO, superhydrophobic nanostructured ZnO (SA coated), and superhydrophobic nanostructured ZnO (FAS coated) samples of size 1 cm^2 were dipped in 10 mL PBS for 3 h. All the experiments were performed in triplicates. In addition, we used only PBS solution as control. After dipping the samples for 3 h in PBS, the samples were taken out. Then, the solutions were diluted 1000× with 2% HNO_3. Finally, the concentrations of Zn^{2+} ions in all the samples were measured based on the standard calibration plot.

3. RESULTS AND DISCUSSION

3.1. Fabrication Strategy. Three types of samples—one superhydrophilic and two superhydrophobic—were prepared with the protocol, as shown in Figure 1. The superhydrophilic sample was composed of nonfunctionalized ZnO nanostructures, obtained in a single fabrication step involving immersion of the zinc substrate in hot water, and maintained at a constant temperature of 95 ± 2 °C, up to 24 h. Similar structuring of various metals using hot water baths has already been shown in the literature.[28,35]

The superhydrophobic samples required a second fabrication step, for hydrophobization. Superhydrophobicity was achieved by following two chemical modification approaches. The first approach involved a fluorine-free process, wherein the samples were immersed in a low concentration ethanolic SA solution. SA is known to produce a chemical bond with ZnO.[46,47] Following the immersion process, an annealing step was performed to achieve a conformal hydrophobic coating over the underlying ZnO nanostructures. The second hydrophobization approach was entirely water-based, where a water-dispersed, readily biodegradable FAS was sprayed on a hot nanostructured zinc substrate, so that the aerosol droplets coming from the sprayed solution evaporated instantly and the FAS was deposited again uniformly atop the ZnO nanostructures. Such waterborne organosilanes have been used on a variety of substrates for hydrophobization and corrosion protection.[48,49]

3.2. Surface Morphology. Figure 2 shows the evolution of ZnO nanostructures, starting from an as-received surface (Figure 2a), as a function of the immersion time in hot water (95 °C).[35,50] The resulting fast adsorption and breakup of the

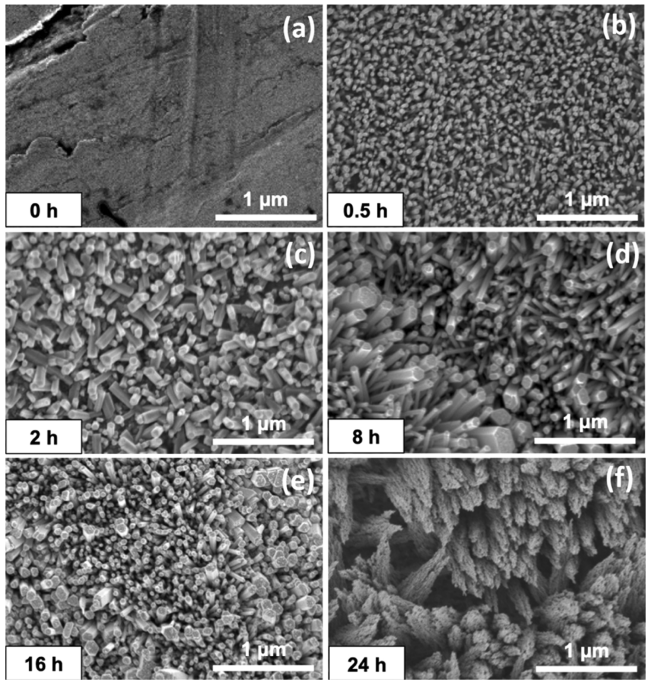

Figure 2. SEM pictures of ZnO nanostructures for increasing time of immersion in the hot water bath process. Starting from an as-received substrate (a), the steps involve the initial growth step of the ZnO nanorods (b), the shape evolution (d,e) into hexagonal nanorods, and the final step of redeposition of ZnO species that enlarges and roughens the existing nanostructures (f).

polar water molecule on the zinc surface accelerates the kinetics of oxidation to form ZnO nanocrystals that serve as a seed for further growth through Zn ion diffusion (Figure 2b). During the initial stage, ZnO nanowire growth occurs because of the preferential diffusion of Zn ions to the tips of the ZnO nanostructures. The ZnO nanocrystals self-arrange in a hexagonal structure. This is because polar faces with surface dipoles (Zn^{2+} or O_2^-) are thermodynamically less stable than nonpolar faces and tend to minimize their surface energy by undergoing rearrangement.[51] This results in the growth of ZnO nanorods with hexagonal tips, which eventually reach a specific size as observed in the time sequences in SEM, as shown in Figure 2c–e. When the ZnO nanowires become too long for Zn ion diffusion to efficiently reach their tips, the

https://dx.doi.org/10.1021/acs.iecr.0c01998
Ind. Eng. Chem. Res. 2020, 59, 14323−14333

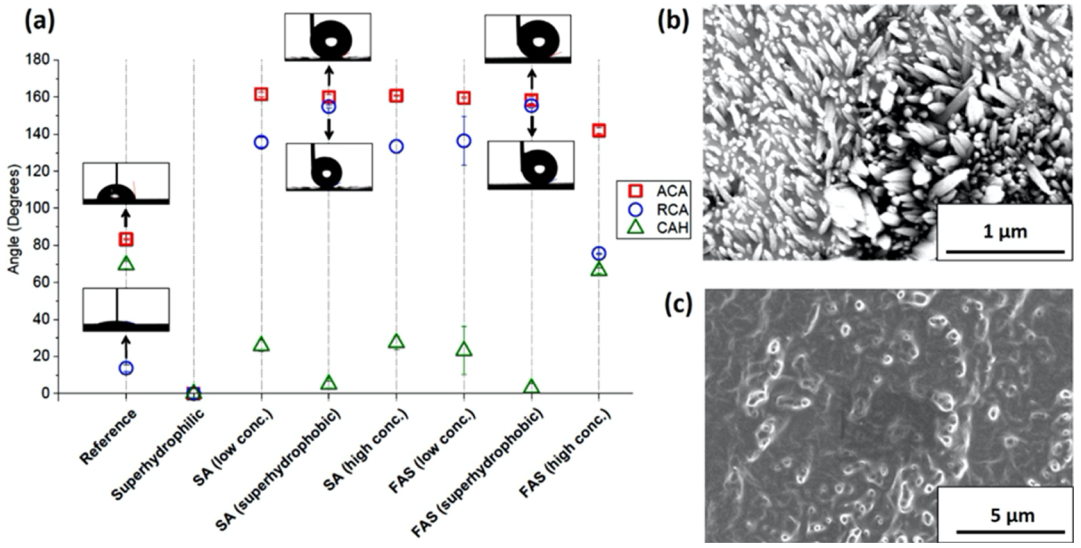

Figure 3. (a) ACA, RCA, and CAH of the different samples under consideration. Low, optimal, and high concentrations for SA are 0.1, 0.38, and 1.4 g/L respectively, while for the FAS, 0.5, 1, and 5 wt %. Insets show water drops during the ACA and RCA measurements of the reference (untreated Zn with native ZnO) sample and the two superhydrophobic treatments with the optimal concentrations. (b) SEM micrograph of a high concentration; SA-coated sample of ZnO nanostructures shows that part of the coating fills the air voids within the nanostructures, thus increasing the water adhesion. (c) Similarly, the SEM micrograph for the FAS-coated sample shows that the ZnO nanostructure morphology is significantly flattened for higher FAS concentration.

formation mechanism changes. At this stage, the dissolution of ZnO results in the formation of hydroxide and $Zn(OH)^+$ at the surface of the specimens. This ionic hydroxide layer is then subsequently dissolved into the hot water bath as the surface of the oxide continues to be hydrolyzed.[52] Next, the solution near the surface eventually becomes supersaturated, and the dissolved hydroxide is redeposited onto the surface, to form ZnO. This phenomenon is observed after a prolonged hot water treatment time (typically around 24 h) when the redeposition of ZnO onto the surface results in coarse nanorod formation (Figure 2f).

3.3. Surface Properties. The wetting properties of the as-received and two superhydrophobic samples are shown in the graph of Figure 3a. The reference Zn sample exhibited an advancing contact angle (ACA) of 83° and CAH of 69°. After boiling, the nanostructured ZnO sample was found to be superhydrophilic, so that contact angles could not be measured as they were approaching the value of 0°. Regarding the two superhydrophobic surface treatments, the concentrations of FAS and SA in their respective solutions were optimized to maximize ACA and minimize CAH, as shown in Figure 3a. The optimal concentrations for SA and FAS resulted in ACA of 160° and CAH of 5° for the case of SA and ACA of 158° and CAH of 3° for the FAS. While concentrations lower than optimal resulted in only partial hydrophobization, higher than optimal concentrations (0.38 g/L SA in ethanol and 1 wt % FAS in water) caused filling of the air voids between the nanostructures, thus flattening the surface. Therefore, surfaces with such concentrations resulted in higher CAH, while still maintaining high ACAs (above 150°). Such behavior of high ACAs accompanied with higher CAH has also been shown in the literature.[53] Examples of surface morphologies after using higher than the optimal concentrations are given in the SEM micrographs of Figure 3b (SA) and 3c (FAS). Figure S1 shows the SEM images with the optimal concentrations on SA and FAS, which look very similar to the ones on Figure 2 which do not have any coating. The only evidence for the coating presence are the wettability measurements and the elemental analysis that we will describe later on. This confirms that with these concentrations, we achieve surface hydrophobization without altering the surface geometry.

To further demonstrate the exceptional superhydrophobic properties of the hydrophobized nanostructures, self-cleaning and condensation experiments were also performed. Self-cleaning experiments were performed by spreading powder on the superhydrophobic surfaces and allowing water drops to roll-off the surfaces while collecting the powder. The contaminant powder was easily removed by the rolling drops, indicating weak adherence of the powder to the surface. Video S1 shows a superhydrophobic-nanostructured ZnO sample coated with SA, but similar results were also obtained with the FAS coating. Materials showing such self-cleaning behavior are known to also exhibit reduced bacterial adhesion.[11] This is the so-called "antifouling" approach, which is considerably different from the "bactericidal" surface concept, as explained earlier.[54]

We also investigated the hydrophobicity of the samples toward small droplets through *in situ* condensation experiments in environmental SEM.[55] The samples demonstrated dropwise condensation, indicating conformal hydrophobization of the nanostructures. It is important to mention here that several superhydrophobic surfaces exhibit hydrophobicity deterioration at small droplet scales, a characteristic example being the Lotus leaf.[56,57] Please refer to Supporting Information Section S1, Figure S2, and Videos S2−S4 for further details on condensation experiments.

Furthermore, we confirmed the surface chemistry of the fabricated samples using energy-dispersive X-ray spectroscopy (EDX). EDX analysis showed increasing concentration of oxygen on the surface with increase in immersion time, thus confirming the nanostructures to be composed of ZnO. The surface elemental maps obtained through EDX analysis confirmed the chemical homogeneity of the surface. Please refer to Supporting Information, Sections S2 and S3, and

https://dx.doi.org/10.1021/acs.iecr.0c01998
Ind. Eng. Chem. Res. 2020, 59, 14323−14333

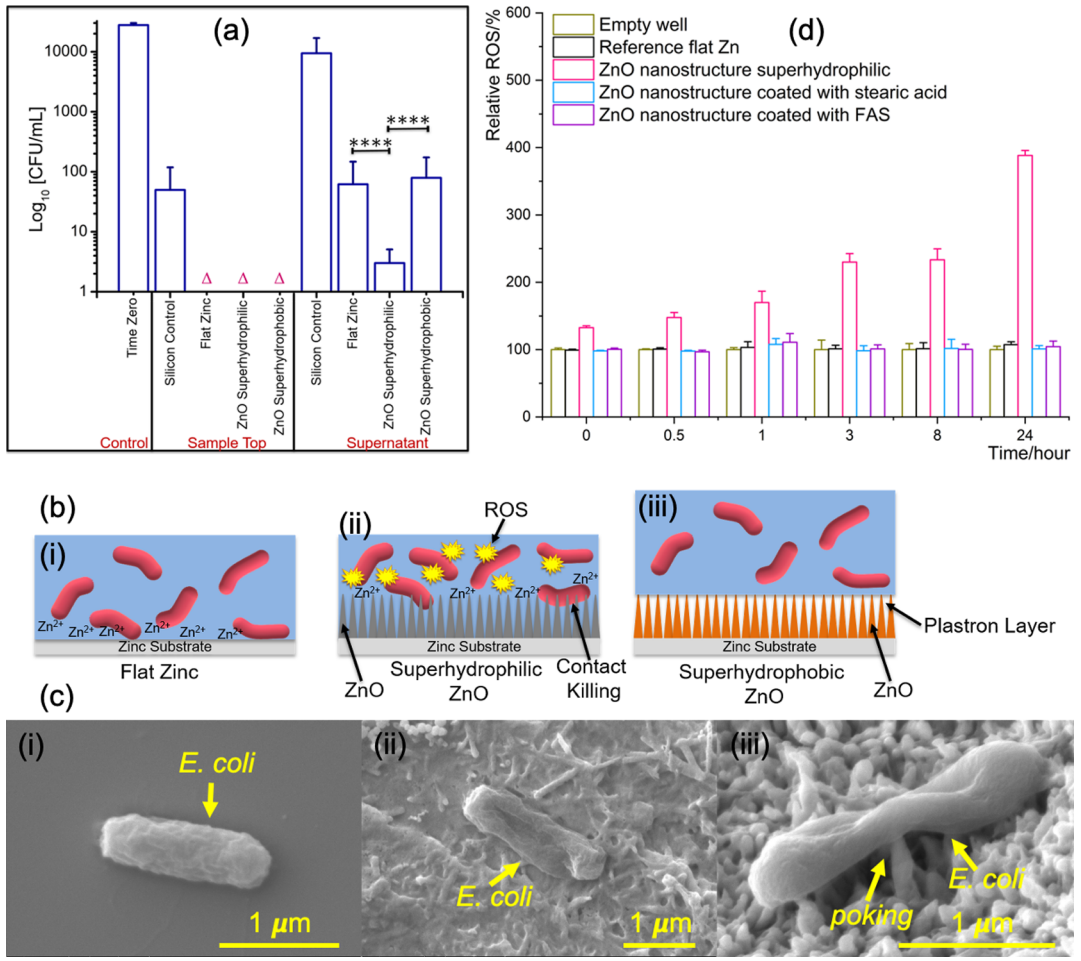

Figure 4. (a) Cell viability of *E. coli* on top of the test substrates and in the supernatant at 0 and 3 h incubation time. "△" Symbol implies that no viable bacterial colony was found. Statistical significance was performed using Student's *t*-test [****$P \leq 0.0001$]. (b) Illustration of the different surface−bacteria interactions on flat Zn substrates, nanostructured superhydrophilic ZnO surfaces, and nanostructured hydrophobized ZnO surfaces. (c) Morphology of *E. coli* on (i) glass coverslip, (ii) flat zinc, and (iii) nanostructured ZnO superhydrophilic surface. (d) Quantification of ROS generated from all the test substrates in the dark using DHR 123 dye.

Figures S3−S6 for further details on EDX analysis and elemental map.

3.4. Antibacterial Performance. The antibacterial activity of the aforementioned samples was evaluated using the classical colony counting method.[45] After each time point of incubating bacteria with the surfaces, bacterial cultures suspended in 0.9% NaCl saline solution were collected from the top of the test samples and the supernatant was plated separately to enumerate the live bacteria (see the Materials and Methods section for details). Figure 4a shows the number of viable cells on the test substrates and in the respective supernatant of the samples. After incubation for 3 h, considerable number of viable bacteria was found on the silicon substrate, which was taken as a control in our experiment. In contrast, no viable bacterium was found on top of the flat zinc, superhydrophilic ZnO, and superhydrophobic (SA-coated)-nanostructured ZnO surfaces. However, the overall antibacterial performance of the three surfaces arises from multiple mechanisms.

As discussed earlier, Zn and ZnO are known to exhibit antibacterial properties.[23,24,58,59] when microbes come in contact to their surface. This is because of the release of zinc ions (Zn^{2+}), as shown schematically in Figure 4b(i,ii) (refer Supporting Information, Section S6, for zinc ion concentration measurements). Additionally, in the case of superhydrophilic ZnO, the sharp edges of the ZnO nanostructures are able to cause puncturing of the cell walls, thus presenting an additional mechanical killing mechanism,[19] as illustrated schematically in Figure 4b(ii). Bactericidal action because of zinc ions and nanostructures is further elucidated by the *in situ* SEM micrographs of bacteria on three surfaces—glass coverslip as the control sample, flat zinc surface, and nanostructured ZnO superhydrophilic surface—as shown in Figure 4c. On the coverslip, the rod shape of *E. coli* was intact, and the bacterial cells appeared healthy without any damage to the cell wall [Figure 4c(i)]. In contrast, the shape of the bacterial cell walls on flat zinc samples was distorted from rod shape and cell walls were rougher [Figure 4c(ii)] implying reduced integrity of the cell wall. This is because of the electrostatic interaction of the released zinc ions[60] with the cell wall at the vicinity of the flat zinc surface. While this weakening effect of zinc ions is retained and even enhanced on the nanostructured ZnO superhydrophilic surface, the sharp nanostructures also cause *E. coli* cells to be deformed. As shown in Figure 4c(iii), the bacteria try to stretch themselves to enhance their surface area in order to settle on the nanostructures. Additionally, poking of the nanostructures into the cell walls is observed. The combined effect of stretching and poking leads to the leakage

https://dx.doi.org/10.1021/acs.iecr.0c01998
Ind. Eng. Chem. Res. 2020, 59, 14323−14333

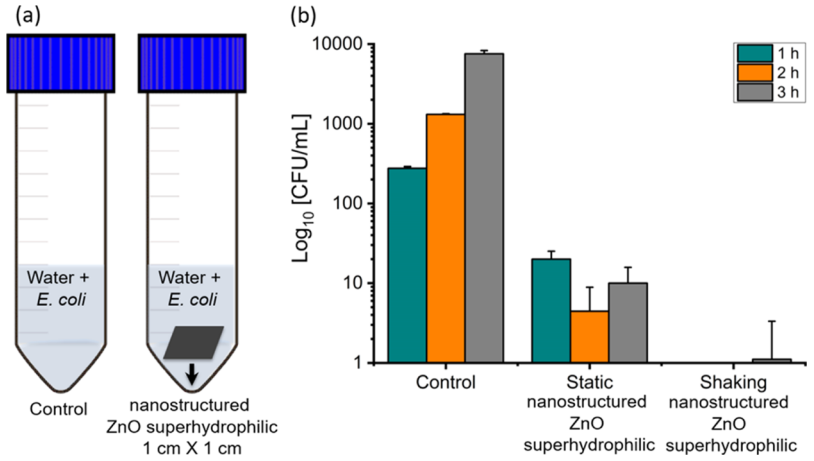

Figure 5. (a) Water disinfection experiment with the nanostructured ZnO surface against Gram-negative *E. coli*. (b) CFU of *E. coli* with and without the nanostructured ZnO surface under static and shaking conditions.

of the intracellular constituents which causes the death of the bacteria on the surface.[61]

The reason that also no viable bacteria were found on the superhydrophobic nanostructured ZnO surface is attributed to the existence of an air plastron layer, as shown schematically in Figure 4b(iii), which provides a cushioning effect preventing the bacteria from adhering to the surface.[62,63] This is further supported by the fact that no bacteria are found in SEM micrographs taken at multiple locations on the superhydrophobic samples [nanostructured ZnO coated with SA (Figure S7a) and nanostructured ZnO coated with FAS (Figure S7b)], which makes the antiadhesion mechanism the only possibility; otherwise, bacterial traces would have been found.[64]

Although flat zinc, superhydrophilic ZnO, and superhydrophobic ZnO surfaces exhibited similar antibacterial performance on top of the surface, the antibacterial efficacy of these substrates to the challenging task of eliminating remote bacteria, that is, bacteria in the supernatant away from the antibacterial surface, was found to be significantly different. Remote live bacteria can further undergo binary fission to increase their colonies. As shown in Figure 4a, in our tests, a considerable number of bacteria was found in the supernatant of silicon, Flat zinc, and nanostructured superhydrophobic ZnO surfaces also showed limited effectiveness in eliminating remote bacteria. Interestingly, however, a significantly smaller (after performing Student's *t*-test) number of bacteria was found in the supernatant of the nanostructured superhydrophilic ZnO surface. We attribute this to the ROS generated from the superhydrophilic ZnO surface. ROS such as the hydroxyl radical, singlet oxygen, and superoxide are strong oxidants and can disinfect pathogens by damaging essential macromolecules.[65,66] Most important advantage of ZnO is that it can generate ROS yielding antibacterial action also in the dark,[67−69] which makes it superior to substrates which require light to generate ROS[43,70] (note that presence of light will also further enhance the ROS generation from ZnO). Atmospheric oxygen can interact with an electron of the ZnO surface forming a superoxide radical ($^{\bullet}O_2^-$). This superoxide reacts with the water molecule to form the hydroperoxyl radical ($^{\bullet}HO_2$), and hydroperoxyl radicals combine with each other to form hydrogen peroxide (H_2O_2). Further, H_2O_2 might react with the superoxide radical to form the hydroxyl ion (OH^-) and hydroxyl radical ($^{\bullet}OH$). This is how ZnO generates ROS under dark condition.

To validate the remote bactericidal effect, the ROS generated from each substrate in dark condition was quantified through fluorescence tests. The corresponding fluorescence data of the blank well, flat zinc sample, nanostructured ZnO samples, nanostructured ZnO coated with SA, and nanostructured ZnO coated with FAS were compared, as shown in Figure 4d. DHR 123 is an uncharged and nonfluorescent ROS indicator. In the presence of ROS, it becomes oxidized to cationic rhodamine 123, which exhibits green fluorescence. Hence, a higher amount of fluorescence implies a higher amount of generated ROS.[71] The nanostructured superhydrophilic ZnO surface produced the highest amount of ROS, as shown in Figure 4d. For the flat zinc surface, ROS generation is lower because of a much smaller surface area available in comparison to nanostructured superhydrophilic ZnO surface. In the case of superhydrophobic surfaces, the two superhydrophobic coatings over the ZnO nanostructures act as barrier layers for the ROS generation. Although we report ROS generation up to 24 h, the results are likely to become even more contrasting for longer duration of exposure of bacterial culture to these surfaces, as the generation of ROS increases with time. In summary, the nanostructured superhydrophilic ZnO surface kills the bacteria present on top of the surface, through release of zinc ions and mechanical poking, as well as remote bacteria in the supernatant through ROS generation, even in complete absence of illumination.

3.5. Water Disinfection. Finally, we employed nanostructured ZnO superhydrophilic surfaces, which exhibited the highest efficacy in inactivating Gram-negative *E. coli*, for water disinfection. For this experiment, 5 mL of distilled (DI) water was placed in each Falcon centrifuge tube and the nanostructured ZnO superhydrophilic samples (grown for 24 h) were placed inside these tubes; 0.5 mL of bacterial suspension in PBS with a concentration of 10^5 CFU/mL was added to each tube containing 5 mL of DI water for both cases, with and without the sample (Figure 5a). The centrifuge tubes containing bacteria and DI water with ZnO samples were incubated under static and shaking conditions (160 rpm, 37 °C) to see the effect of mechanical agitation on the antibacterial performance of the ZnO samples. Figure 5b shows the water disinfection efficacy of the nanostructured ZnO superhydrophilic samples under static and shaking

https://dx.doi.org/10.1021/acs.iecr.0c01998
Ind. Eng. Chem. Res. 2020, 59, 14323−14333

conditions. The results were compared with the control centrifuge tubes without ZnO samples. In dark conditions, the nanostructured ZnO surface exhibited efficient water disinfection behavior under both static and shaking conditions. After 3 h of incubation, we observed three orders of magnitude reduction under static conditions and four orders of magnitude reduction under shaking conditions of the bacterial colonies compared to the control. The efficient water disinfection behavior of the nanostructured ZnO surface is attributed to the ROS generated from the surface (Figure 4b). We also measured the Zn^{2+} ion concentration in the PBS medium released from the bare nanostructured ZnO surface. Inductively couple plasma mass spectroscopy (ICP−MS) was used to measure the Zn^{2+} ion concentration (see the Materials and Methods section for details). The Zn^{2+} ion concentration was found to be 0.73 ± 0.15 ppm which is way below the health limit stated by the World Health Organization (WHO) for safe drinking water (5−6 ppm).[72] The same applies also for the rest of the samples (see Section S6 in the Supporting Information). Hence, the water after disinfection is safe to drink. In this water disinfection method, we propose that the inactivation of bacteria by ROS is the dominant mechanism as the concentration of the Zn^{2+} ions is lower than the minimum inhibitory concentration required to kill bacteria.[21,73,74] Bare nanostructured ZnO surface can be potentially utilized to efficiently disinfect water contaminated with different kinds of microbes in remote and developing areas of the world, where other effective means of water disinfection are not available. The uniqueness of this approach lies in its ability to generate ROS even at dark conditions (a main limitation of the popular SODIS method[41]) combined with the facile surface fabrication based on a fully environmentally benign process. This implies that our approach can be used to continuously disinfect drinking water without any stoppages during cloudy weather or during night, thus marking a significant advance over the state of the art.

4. CONCLUSIONS

We have demonstrated a two-pronged, ZnO-based, facile, and environmentally benign approach for achieving controlled antibacterial action, inhibiting bacterial contamination on surfaces and/or disinfecting contaminated water. The resulting surfaces are characterized for wettability, topology of surface texture, and chemical homogeneity. We have shown that the superhydrophobic ZnO substrates exhibit significant self-cleaning properties and thus have the ability toward minimal bacterial adhesion and, hence, inhibition of surface bacterial contamination. We have also shown that the bare nanostructured ZnO exhibit excellent bactericidal action, killing bacteria both in contact and remotely and most importantly without requiring any illumination. The possibility of controlling the antibacterial behavior together with the upscaling capability and the absence of strong acids, as well as flammable and toxic liquids in the "green" material preparation protocols, render this approach attractive for use in a host of related applications.

■ ASSOCIATED CONTENT

Supporting Information

The Supporting Information is available free of charge at https://pubs.acs.org/doi/10.1021/acs.iecr.0c01998.

SEM images of the hydrophobic samples with optimal concentration, environmental SEM condensation images on nanostructured samples with and without hydrophobization, graphic obtained with EDX analysis, showing the elemental composition of a reference zinc sample, graphic obtained with EDX analysis, showing the elemental composition of a nanostructured ZnO sample, graphic obtained with EDX analysis, showing the elemental composition of a nanostructured ZnO sample coated with 1 wt % FAS solution, elemental map of the carbon, fluorine, oxygen, and zinc on the surface of a nanostructured sample, coated with 1 wt % FAS solution, SEM images of superhydrophobic samples after incubation, and Zn ion concentration for all samples (PDF)

Video of the self-cleaning experiment (AVI)

Condensation on the reference untreated sample (AVI)

Condensation on the superhydrophobic nanostructured sample coated with SA (AVI)

Condensation on the superhydrophobic nanostructured sample coated with FAS (AVI)

■ AUTHOR INFORMATION

Corresponding Author

Dimos Poulikakos − *Laboratory of Thermodynamics in Emerging Technologies, Department of Mechanical and Process Engineering, ETH Zürich, 8092 Zürich, Switzerland;* orcid.org/0000-0001-5733-6478; Email: dpoulikakos@ethz.ch

Authors

Athanasios Milionis − *Laboratory of Thermodynamics in Emerging Technologies, Department of Mechanical and Process Engineering, ETH Zürich, 8092 Zürich, Switzerland;* orcid.org/0000-0002-0049-1255

Abinash Tripathy − *Laboratory of Thermodynamics in Emerging Technologies, Department of Mechanical and Process Engineering, ETH Zürich, 8092 Zürich, Switzerland;* orcid.org/0000-0003-3546-2806

Matteo Donati − *Laboratory of Thermodynamics in Emerging Technologies, Department of Mechanical and Process Engineering, ETH Zürich, 8092 Zürich, Switzerland;* orcid.org/0000-0003-0197-0159

Chander Shekhar Sharma − *Laboratory of Thermodynamics in Emerging Technologies, Department of Mechanical and Process Engineering, ETH Zürich, 8092 Zürich, Switzerland;* orcid.org/0000-0002-6193-6457

Fei Pan − *Laboratory for Biointerfaces, Empa, Swiss Federal Laboratories for Materials Science and Technology, 9014 St. Gallen, Switzerland;* orcid.org/0000-0002-9801-5619

Katharina Maniura-Weber − *Laboratory for Biointerfaces, Empa, Swiss Federal Laboratories for Materials Science and Technology, 9014 St. Gallen, Switzerland;* orcid.org/0000-0001-7895-3563

Qun Ren − *Laboratory for Biointerfaces, Empa, Swiss Federal Laboratories for Materials Science and Technology, 9014 St. Gallen, Switzerland;* orcid.org/0000-0003-0627-761X

Complete contact information is available at: https://pubs.acs.org/10.1021/acs.iecr.0c01998

Author Contributions

§A.M. and A.T. contributed equally to this work.

Funding

This project has received funding from the European Union's Horizon 2020 research and innovation programme under grant number 801229 (HARMoNIC), the ERC Advanced Grant (grant no. 669908 INTICE), and the Commission for Technology and Innovation, (CTI) under the Swiss Competence Centers for Energy Research (SCCER) programme (grant no. KTI.2014.0148).

Notes

The authors declare no competing financial interest.

■ ACKNOWLEDGMENTS

We thank Ms. Flavia Zuver for her help in the antibacterial experiments and Dr. Corey Archer for the Zinc ion concentration measurement.

■ ABBREVIATIONS

FAS	fluoroalkylsilane
SA	stearic acid
HAI	healthcare associated infection
ROS	reactive oxygen species
SODIS	solar water disinfection
ACA	advancing contact angle
CAH	contact angle hysteresis
RCA	receding contact angle
ESEM	environmental scanning electron microscope
EDX	energy-dispersive X-ray spectroscopy
CFU	colony forming units
DHR	dihydrorhodamine
PBS	phosphate-buffered saline

■ REFERENCES

(1) World Health Organization. *Health Care-Associated Infections Fact Sheet*; World Health Organization, 2015, p 4.
(2) Nurain, A. M.; Bilal, N. E.; Ibrahim, M. E. The Frequency and Antimicrobial Resistance Patterns of Nosocomial Pathogens Recovered from Cancer Patients and Hospital Environments. *Asian Pac. J. Trop. Biomed.* **2015**, *5*, 1055−1059.
(3) Chen, L.-K.; Kuo, S.-C.; Chang, K.-C.; Cheng, C.-C.; Yu, P.-Y.; Chang, C.-H.; Chen, T.-Y.; Tseng, C.-C. Clinical Antibiotic-Resistant Acinetobacter Baumannii Strains with Higher Susceptibility to Environmental Phages than Antibiotic-Sensitive Strains. *Sci. Rep.* **2017**, *7*, 6319.
(4) Seigal, A.; Mira, P.; Sturmfels, B.; Barlow, M. Does Antibiotic Resistance Evolve in Hospitals? *Bull. Math. Biol.* **2017**, *79*, 191−208.
(5) Seidl, K.; Leimer, N.; Palheiros Marques, M.; Furrer, A.; Holzmann-Bürgel, A.; Senn, G.; Zbinden, R.; Zinkernagel, A. S. Clonality and Antimicrobial Susceptibility of Methicillin-Resistant Staphylococcus Aureus at the University Hospital Zurich, Switzerland between 2012 and 2014. *Ann. Clin. Microbiol. Antimicrob.* **2015**, *14*, 14.
(6) Wiggli, B. J.; Frei, R.; Laffer, R.; Tschudin Sutter, S.; Widmer, A. F. Survival from Methicillin-Sensitive Staphylococcus Aureus Bloodstream Infections over 20 Years: A Cohort of 1328 Patients. *Swiss Med. Wkly.* **2017**, *147*, w14508.
(7) Cohen, P. R.; Kurzrock, R. Community-Acquired Methicillin-Resistant Staphylococcus Aureus Skin Infection: An Emerging Clinical Problem. *J. Am. Acad. Dermatol.* **2004**, *50*, 277−280.
(8) Stryjewski, M. E.; Corey, G. R. Methicillin-Resistant Staphylococcus Aureus: An Evolving Pathogen. *Clin. Infect. Dis.* **2014**, *58*, 10−19.
(9) World Health Organization. *WHO 2.1 Billion People Lack Safe Drinking Water at Home, More than Twice as Many Lack Safe Sanitation*. Un 2017, July 2−5.
(10) Ramírez-Castillo, F.; Loera-Muro, A.; Jacques, M.; Garneau, P.; Avelar-González, F.; Harel, J.; Guerrero-Barrera, A. Waterborne Pathogens: Detection Methods and Challenges. *Pathogens* **2015**, *4*, 307−334.
(11) Ellinas, K.; Kefallinou, D.; Stamatakis, K.; Gogolides, E.; Tserepi, A. Is There a Threshold in the Antibacterial Action of Superhydrophobic Surfaces? *ACS Appl. Mater. Interfaces* **2017**, *9*, 39781−39789.
(12) Li, Z.; Milionis, A.; Zheng, Y.; Yee, M.; Codispoti, L.; Tan, F.; Poulikakos, D.; Yap, C. H. Superhydrophobic Hemostatic Nanofiber Composites for Fast Clotting and Minimal Adhesion. *Nat. Commun.* **2019**, *10*, 5562.
(13) Barthlott, W.; Neinhuis, C. Purity of the Sacred Lotus, or Escape from Contamination in Biological Surfaces. *Planta* **1997**, *202*, 1−8.
(14) Milionis, A.; Sharma, C. S.; Hopf, R.; Uggowitzer, M.; Bayer, I. S.; Poulikakos, D. Engineering Fully Organic and Biodegradable Superhydrophobic Materials. *Adv. Mater. Interfaces* **2019**, *6*, 1801202.
(15) Milionis, A.; Giannuzzi, R.; Bayer, I. S.; Papadopoulou, E. L.; Ruffilli, R.; Manca, M.; Athanassiou, A. Self-Cleaning Organic/Inorganic Photo-Sensors. *ACS Appl. Mater. Interfaces* **2013**, *5*, 7139−7145.
(16) Tripathy, A.; Sen, P.; Su, B.; Briscoe, W. H. Natural and Bioinspired Nanostructured Bactericidal Surfaces. *Adv. Colloid Interface Sci.* **2017**, *248*, 85−104.
(17) Tripathy, A.; Sreedharan, S.; Bhaskarla, C.; Majumdar, S.; Peneti, S. K.; Nandi, D.; Sen, P. Enhancing the Bactericidal Efficacy of Nanostructured Multifunctional Surface Using an Ultrathin Metal Coating. *Langmuir* **2017**, *33*, 12569−12579.
(18) Tripathy, A.; Pahal, S.; Mudakavi, R. J.; Raichur, A. M.; Varma, M. M.; Sen, P. Impact of Bioinspired Nanotopography on the Antibacterial and Antibiofilm Efficacy of Chitosan. *Biomacromolecules* **2018**, *19*, 1340−1346.
(19) Ivanova, E. P.; Hasan, J.; Webb, H. K.; Truong, V. K.; Watson, G. S.; Watson, J. A.; Baulin, V. A.; Pogodin, S.; Wang, J. Y.; Tobin, M. J.; et al. Natural Bactericidal Surfaces: Mechanical Rupture of Pseudomonas Aeruginosa Cells by Cicada Wings. *Small* **2012**, *8*, 2489−2494.
(20) Jiang, J.; Pi, J.; Cai, J. The Advancing of Zinc Oxide Nanoparticles for Biomedical Applications. *Bioinorg. Chem. Appl.* **2018**, *2018*, 1−18.
(21) Fiedot, M.; Maliszewska, I.; Rac-Rumijowska, O.; Suchorska-Woźniak, P.; Lewínska, A.; Teterycz, H. The Relationship between the Mechanism of Zinc Oxide Crystallization and Its Antimicrobial Properties for the Surface Modification of Surgical Meshes. *Materials* **2017**, *10*, 353.
(22) Pasquet, J.; Chevalier, Y.; Pelletier, J.; Couval, E.; Bouvier, D.; Bolzinger, M.-A. The Contribution of Zinc Ions to the Antimicrobial Activity of Zinc Oxide. *Colloids Surf., A* **2014**, *457*, 263−274.
(23) McDevitt, C. A.; Ogunniyi, A. D.; Valkov, E.; Lawrence, M. C.; Kobe, B.; McEwan, A. G.; Paton, J. C. A Molecular Mechanism for Bacterial Susceptibility to Zinc. *PLoS Pathog.* **2011**, *7*, No. e1002357.
(24) Kadiyala, U.; Turali-Emre, E. S.; Bahng, J. H.; Kotov, N. A.; VanEpps, J. S. Unexpected Insights into Antibacterial Activity of Zinc Oxide Nanoparticles against Methicillin Resistant: Staphylococcus Aureus (MRSA). *Nanoscale* **2018**, *10*, 4927−4939.
(25) Almoudi, M. M.; Hussein, A. S.; Abu Hassan, M. I.; Mohamad Zain, N. A Systematic Review on Antibacterial Activity of Zinc against Streptococcus Mutans. *Saudi Dent. J.* **2018**, *30*, 283−291.
(26) Qian, B.; Shen, Z. Fabrication of Superhydrophobic Surfaces by Dislocation-Selective Chemical Etching on Aluminum, Copper, and Zinc Substrates. *Langmuir* **2005**, *21*, 9007−9009.
(27) Jana, T. K.; Jana, S. K.; Kumar, A.; De, K.; Maiti, R.; Mandal, A. K.; Chatterjee, T.; Chatterjee, B. K.; Chakrabarti, P.; Chatterjee, K. The Antibacterial and Anticancer Properties of Zinc Oxide Coated Iron Oxide Nanotextured Composites. *Colloids Surf., B* **2019**, *177*, 512−519.
(28) Sharma, C. S.; Combe, J.; Giger, M.; Emmerich, T.; Poulikakos, D. Growth Rates and Spontaneous Navigation of Condensate

https://dx.doi.org/10.1021/acs.iecr.0c01998
Ind. Eng. Chem. Res. 2020, 59, 14323−14333

Droplets Through Randomly Structured Textures. *ACS Nano* **2017**, *11*, 1673−1682.
(29) Huang, Q.; Yang, Y.; Hu, R.; Lin, C.; Sun, L.; Vogler, E. A. Reduced Platelet Adhesion and Improved Corrosion Resistance of Superhydrophobic TiO2-Nanotube-Coated 316L Stainless Steel. *Colloids Surf., B* **2015**, *125*, 134−141.
(30) Milionis, A.; Dang, K.; Prato, M.; Loth, E.; Bayer, I. S. Liquid Repellent Nanocomposites Obtained from One-Step Water-Based Spray. *J. Mater. Chem. A* **2015**, *3*, 12880−12889.
(31) Dong, Z.; Ma, J.; Jiang, L. Manipulating and Dispensing Micro/Nanoliter Droplets by Superhydrophobic Needle Nozzles. *ACS Nano* **2013**, *7*, 10371−10379.
(32) Vercillo, V.; Cardoso, J. T.; Huerta-Murillo, D.; Tonnicchia, S.; Laroche, A.; Mayén Guillén, J. A.; Ocaña, J. L.; Lasagni, A. F.; Bonaccurso, E. Durability of Superhydrophobic Laser-Treated Metal Surfaces under Icing Conditions. *Mater. Lett. X* **2019**, *3*, 100021.
(33) Liu, C.; Gin, K. Y. H.; Chang, V. W. C.; Goh, B. P. L.; Reinhard, M. Novel Perspectives on the Bioaccumulation of PFCs - The Concentration Dependency. *Environ. Sci. Technol.* **2011**, *45*, 9758−9764.
(34) Higgins, C. P.; Mcleod, P. B.; Macmanus-Spencer, L. A.; Luthy, R. G. Bioaccumulation of Perfluorochemicals in Sediments by the Aquatic Oligochaete Lumbriculus Variegatus. *Environ. Sci. Technol.* **2007**, *41*, 4600−4606.
(35) Saadi, N. S.; Hassan, L. B.; Karabacak, T. Metal Oxide Nanostructures by a Simple Hot Water Treatment. *Sci. Rep.* **2017**, *7*, 7158.
(36) Khedir, K. R.; Saifaldeen, Z. S.; Demirkan, T. M.; Al-Hilo, A. A.; Brozak, M. P.; Karabacak, T. Robust Superamphiphobic Nanoscale Copper Sheet Surfaces Produced by a Simple and Environmentally Friendly Technique. *Adv. Eng. Mater.* **2015**, *17*, 982−989.
(37) Saifaldeen, Z. S.; Khedir, K. R.; Cansizoglu, M. F.; Demirkan, T.; Karabacak, T. Superamphiphobic Aluminum Alloy Surfaces with Micro and Nanoscale Hierarchical Roughness Produced by a Simple and Environmentally Friendly Technique. *J. Mater. Sci.* **2014**, *49*, 1839−1853.
(38) Liu, K.; Jiang, L. Metallic Surfaces with Special Wettability. *Nanoscale* **2011**, *3*, 825.
(39) Mates, J. E.; Schutzius, T. M.; Bayer, I. S.; Qin, J.; Waldroup, D. E.; Megaridis, C. M. Water-Based Superhydrophobic Coatings for Nonwoven and Cellulosic Substrates. *Ind. Eng. Chem. Res.* **2014**, *53*, 222−227.
(40) Zhou, H.; Wang, H.; Niu, H.; Zhao, Y.; Xu, Z.; Lin, T. A Waterborne Coating System for Preparing Robust, Self-Healing, Superamphiphobic Surfaces. *Adv. Funct. Mater.* **2017**, *27*, 1604261.
(41) McGuigan, K. G.; Conroy, R. M.; Mosler, H.-J.; Preez, M. d.; Ubomba-Jaswa, E.; Fernandez-Ibañez, P. Solar Water Disinfection (SODIS): A Review from Bench-Top to Roof-Top. *J. Hazard. Mater.* **2012**, *235*−*236*, 29−46.
(42) Karran, P.; Brem, R. Protein Oxidation, UVA and Human DNA Repair. *DNA Repair* **2016**, *44*, 178−185.
(43) Liu, C.; Kong, D.; Hsu, P.-C.; Yuan, H.; Lee, H.-W.; Liu, Y.; Wang, H.; Wang, S.; Yan, K.; Lin, D.; et al. Rapid Water Disinfection Using Vertically Aligned MoS 2 Nanofilms and Visible Light. *Nat. Nanotechnol.* **2016**, *11*, 1098−1104.
(44) Rykaczewski, K.; Scott, J. H. J.; Fedorov, A. G. Electron Beam Heating Effects during Environmental Scanning Electron Microscopy Imaging of Water Condensation on Superhydrophobic Surfaces. *Appl. Phys. Lett.* **2011**, *98*, 093106.
(45) Sanders, E. R. Aseptic Laboratory Techniques: Plating Methods. *J. Visualized Exp.* **2012**, *63*, No. e3064.
(46) Wan, Y.; Wang, Z.; Liu, Y.; Qi, C.; Zhang, J. Reducing Friction and Wear of a Zinc Substrate by Combining a Stearic Acid Overcoat with a Nanostructured Zinc Oxide Underlying Film: Perspectives to Super-Hydrophobicity. *Tribol. Lett.* **2011**, *44*, 329−333.
(47) Gurav, A. B.; Latthe, S. S.; Vhatkar, R. S.; Lee, J.-G.; Kim, D.-Y.; Park, J.-J.; Yoon, S. S. Superhydrophobic Surface Decorated with Vertical ZnO Nanorods Modified by Stearic Acid. *Ceram. Int.* **2014**, *40*, 7151−7160.
(48) Fedel, M.; Olivier, M.; Poelman, M.; Deflorian, F.; Rossi, S.; Druart, M.-E. Corrosion Protection Properties of Silane Pre-Treated Powder Coated Galvanized Steel. *Prog. Org. Coat.* **2009**, *66*, 118−128.
(49) Pagliaro, M.; Ciriminna, R.; Palmisano, G. Silica-Based Hybrid Coatings. *J. Mater. Chem.* **2009**, *19*, 3116−3126.
(50) Tan, W. K.; Abdul Razak, K.; Lockman, Z.; Kawamura, G.; Muto, H.; Matsuda, A. Formation of Highly Crystallized ZnO Nanostructures by Hot-Water Treatment of Etched Zn Foils. *Mater. Lett.* **2013**, *91*, 111−114.
(51) Umar, A.; Al-Hajry, A.; Hahn, Y. B.; Kim, D. H. Rapid Synthesis and Dye-Sensitized Solar Cell Applications of Hexagonal-Shaped ZnO Nanorods. *Electrochim. Acta* **2009**, *54*, 5358−5362.
(52) Degen, A.; Kosec, M. Effect of PH and Impurities on the Surface Charge of Zinc Oxide in Aqueous Solution. *J. Eur. Ceram. Soc.* **2000**, *20*, 667−673.
(53) Cheng, Z.; Du, M.; Lai, H.; Zhang, N.; Sun, K. From Petal Effect to Lotus Effect: A Facile Solution Immersion Process for the Fabrication of Super-Hydrophobic Surfaces with Controlled Adhesion. *Nanoscale* **2013**, *5*, 2776−2783.
(54) Hasan, J.; Crawford, R. J.; Ivanova, E. P. Antibacterial Surfaces: The Quest for a New Generation of Biomaterials. *Trends Biotechnol.* **2013**, *31*, 295−304.
(55) Rykaczewski, K.; Paxson, A. T.; Anand, S.; Chen, X.; Wang, Z.; Varanasi, K. K. Multimode Multidrop Serial Coalescence Effects during Condensation on Hierarchical Superhydrophobic Surfaces. *Langmuir* **2013**, *29*, 881−891.
(56) Cheng, Y.-T.; Rodak, D. E. Is the Lotus Leaf Superhydrophobic? *Appl. Phys. Lett.* **2005**, *86*, 144101.
(57) Boreyko, J. B.; Chen, C.-H. Restoring Superhydrophobicity of Lotus Leaves with Vibration-Induced Dewetting. *Phys. Rev. Lett.* **2009**, *103*, 184501.
(58) Rago, I.; Chandraiahgari, C. R.; Bracciale, M. P.; De Bellis, G.; Zanni, E.; Cestelli Guidi, M.; Sali, D.; Broggi, A.; Palleschi, C.; Sarto, M. S.; et al. Zinc Oxide Microrods and Nanorods: Different Antibacterial Activity and Their Mode of Action against Gram-Positive Bacteria. *RSC Adv.* **2014**, *4*, 56031−56040.
(59) Tripathy, A.; Wąsik, P.; Sreedharan, S.; Nandi, D.; Bikondoa, O.; Su, B.; Sen, P.; Briscoe, W. H. Facile Fabrication of Multifunctional ZnO Urchins on Surfaces. *Colloids Interfaces* **2018**, *2*, 74.
(60) Siddiqi, K. S.; ur Rahman, A.; Tajuddin; Husen, A. Properties of Zinc Oxide Nanoparticles and Their Activity Against Microbes. *Nanoscale Res. Lett.* **2018**, *13*, 141.
(61) Ivanova, E. P.; Hasan, J.; Webb, H. K.; Gervinskas, G.; Juodkazis, S.; Truong, V. K.; Wu, A. H. F.; Lamb, R. N.; Baulin, V. A.; Watson, G. S.; et al. Bactericidal Activity of Black Silicon. *Nat. Commun.* **2013**, *4*, 2838.
(62) Hwang, G. B.; Page, K.; Patir, A.; Nair, S. P.; Allan, E.; Parkin, I. P. The Anti-Biofouling Properties of Superhydrophobic Surfaces Are Short-Lived. *ACS Nano* **2018**, *12*, 6050−6058.
(63) Zhang, X.; Wang, L.; Levänen, E. Superhydrophobic Surfaces for the Reduction of Bacterial Adhesion. *RSC Adv.* **2013**, *3*, 12003.
(64) Hizal, F.; Rungraeng, N.; Lee, J.; Jun, S.; Busscher, H. J.; Van Der Mei, H. C.; Choi, C.-H. Nanoengineered Superhydrophobic Surfaces of Aluminum with Extremely Low Bacterial Adhesivity. *ACS Appl. Mater. Interfaces* **2017**, *9*, 12118−12129.
(65) Malato, S.; Fernández-Ibáñez, P.; Maldonado, M. I.; Blanco, J.; Gernjak, W. Decontamination and Disinfection of Water by Solar Photocatalysis: Recent Overview and Trends. *Catal. Today* **2009**, *147*, 1−59.
(66) Chong, M. N.; Jin, B.; Chow, C. W. K.; Saint, C. Recent Developments in Photocatalytic Water Treatment Technology: A Review. *Water Res.* **2010**, *44*, 2997−3027.
(67) Lakshmi Prasanna, V.; Vijayaraghavan, R. Insight into the Mechanism of Antibacterial Activity of ZnO: Surface Defects Mediated Reactive Oxygen Species Even in the Dark. *Langmuir* **2015**, *31*, 9155−9162.

https://dx.doi.org/10.1021/acs.iecr.0c01998
Ind. Eng. Chem. Res. 2020, 59, 14323−14333

(68) Janotti, A.; Van de Walle, C. G. Fundamentals of Zinc Oxide as a Semiconductor. *Rep. Prog. Phys.* **2009**, *72*, 126501.
(69) Jones, N.; Ray, B.; Ranjit, K. T.; Manna, A. C. Antibacterial Activity of ZnO Nanoparticle Suspensions on a Broad Spectrum of Microorganisms. *FEMS Microbiol. Lett.* **2008**, *279*, 71−76.
(70) Yu, J. C.; Ho, W.; Yu, J.; Yip, H.; Wong, P. K.; Zhao, J. Efficient Visible-Light-Induced Photocatalytic Disinfection on Sulfur-Doped Nanocrystalline Titania. *Environ. Sci. Technol.* **2005**, *39*, 1175−1179.
(71) Tan, S.; Sagara, Y.; Liu, Y.; Maher, P.; Schubert, D.; Maher, P. The Regulation of Reactive Oxygen Species Production during Programmed Cell Death. *J. Cell Biol.* **2002**, *141*, 1423−1432.
(72) World Health Organization. Chemical Fact Sheets. *Guidelines for Drinking-Water Quality*, 2010, Chapter 1, pp 296−461.
(73) Fan, W.; Sun, Q.; Li, Y.; Tay, F. R.; Fan, B. Synergistic Mechanism of Ag+-Zn2+ in Anti-Bacterial Activity against Enterococcus Faecalis and Its Application against Dentin Infection. *J. Nanobiotechnol.* **2018**, *16*, 10.
(74) Sirelkhatim, A.; Mahmud, S.; Seeni, A.; Kaus, N. H. M.; Ann, L. C.; Bakhori, S. K. M.; Hasan, H.; Mohamad, D. Review on Zinc Oxide Nanoparticles: Antibacterial Activity and Toxicity Mechanism. *Nano-Micro Lett.* **2015**, *7*, 219−242.

https://dx.doi.org/10.1021/acs.iecr.0c01998
Ind. Eng. Chem. Res. 2020, 59, 14323−14333